Very High Cycle Fatigue for single phase ductile materials: slip band appearance criterion

Ngoc Lam Phung, Nicolas Marti, Antoine Blanche, Nicolas Ranc, Véronique Favier, André Chrysochoos, Nicolas Saintier, Fabienne Gregori, Brigitte Bacroix, Guillaume Thoquenne

5th Fatigue Design Conference, Fatigue Design 2013

Very High Cycle Fatigue for single phase ductile materials: slip band appearance criterion

Ngoc Lam Phung[1], Nicolas Marti[1,3-4], Antoine Blanche[2], Nicolas Ranc[1], Véronique Favier[1*], André Chrysochoos[2], N. Saintier[3], Fabienne Grégori[4] , Brigitte Bacroix[4], Guillaume Thoquenne[5]

[1]*Arts et Métiers ParisTech, PIMM UMR 8006, 75013 Paris, France*
[2]*Montpellier II University, LMGC UMR 5508, France*
[3]*Arts et Métiers ParisTech, I2M UMR 8006, 33607 Bordeaux, France*
[4]*Paris 13 University LSPM UPR 3407, France*
[5]*Cetim, Senlis, France*
* *Corresponding author: veronique.favier@ensam.eu*

Abstract

The DISFAT project is a French project financially supported by the French National Agency for Research (ANR). It aims at a deeper understanding of mechanisms leading to crack initiation in metals and alloys under Very High Cycle Fatigue loading (VHCF). The VHCF regime is associated with stress magnitudes lower than the conventional fatigue limit and as a result, numbers of cycles higher than 10^9. Tests were carried out using an ultrasonic technique at loading frequency of 20 kHz. In the case of pure copper polycrystals, we previously showed that slip band (SB) activity and intrinsic dissipation were closely related. Dissipation and slip band amount increased with the number of cycles. At very small stress amplitudes, no slip band appeared at the specimen surface up to 10^8 cycles but the material was found to dissipate energy. These results revealed that the material never reached a steady state and so could break at higher number of cycles. In this paper, the morphology and the location of slip bands were characterized. Different types of slip bands depending on the stress amplitudes appeared at the specimen surface. The stress amplitude required to show the first slip bands decreases with the number of cycles. It is twice lower than the stress amplitude required to break the specimen for the same number of cycles. At the smallest stress amplitudes, slip bands were mostly found at twin boundaries. Quasi 3D finite element simulations taking into account the polycrystalline nature of the material emphasized the key role of the elastic anisotropy in slip band initiation. A criterion for slip band appearance was finally proposed.

Keywords : Very high cycle fatigue – VHCF ; slip band ; anisotropic elastic crystallinne ; finite element.

1. Introduction

The VHCF regime is associated with stress amplitudes lower than the conventional fatigue limit and as a result, numbers of cycles higher than 10^9. The present project is a fundamental research project. However, it is motivated by industrial problems. Some mechanical components, such as pistons, rotating axes, in the transportation and more generally engineering industry, have been designed previously using fatigue resistance data at lower numbers of cycles ($<10^7$ cycles ; the regime of High Cycle Fatigue, HCF) whereas they must endure cyclic loading for a number of cycles higher than $>10^9$ cycles [1]. Many experiments in the literature prove that failure occurs at stress amplitudes lower than the conventional fatigue limit. There is also growing demand for the development of robust life prediction and damage assessment methodologies that allow the safe extension of service lifetimes for transportation and power generation systems beyond their original design lifetimes; the methodologies must also allow the design of new efficient systems intended to operate at even longer lifetimes.

In the High Cycle Fatigue (HCF), much work, including analyzing and modeling proposed by Pr. H. Mughrabi [2-3] has been performed, and a fair understanding has emerged over the years. Cyclic strain localization in Persistent Slip Bands (PSBs) is generally observed and accepted as the critical onset of fatigue damage in the HCF regime in ductile single-phase materials and also in many precipitation-hardened alloys. Once formed, PSBs, accompanied by the development of extrusions and notch-like deepenings, commonly referred to intrusions, lead to cracks. For ductile single-phase materials, referred as type I materials, only few investigations (mainly on copper [4-9]) are available regarding the shape of the fatigue life curve and the damage evolution. From these experiments, it is suggested that crack initiation takes place at the surface owing to the accumulation of very small but irreversible plastic deformation over very large number of cycles [10]. However, there is no possibility for the formation of a pronounced PSB structure at very low stress amplitudes below the ”PSB threshold” (associated with the HCF regime). Therefore, it is necessary to conduct systematic investigations of type I materials after cyclic deformation in the VHCF regime in order to clarify the role of the above mentioned mechanisms and parameters.

In this work, we focused on pure copper which is face-centered cubic (fcc) single-phase metal. This material is a good candidate because its HCF behavior has been largely studied in literature. To perform experiments up to a very high number of cycles in a reasonable time, ultrasonic equipment at a testing frequency of 20 kHz was used. It takes only fourteen hours to perform 10^9 cycles at a testing frequency of 20 kHz, whereas it takes one hundred days at 100 Hz. The main objective is to characterize the earliest signs of plasticity, i.e. the appearance of the earliest slip markings (SMs) (associated with slip bands (SBs)) on the specimen surface. Their evolution with stress amplitude and with number of cycles was also investigated. The evolution of the intrinsic dissipation with the stress amplitudes was estimated. Quasi 3D finite element simulations taking into account the polycrystalline nature of the material were performed to investigate the role of the elastic anisotropy in slip band appearance as suggested by [11-13]. A special attention was paid to the role of grain orientation and of the initial surface state following the work of Mareau and Favier et al [14-15] in HCF regime.

2. Material and experimental procedure

2.1. Material and specimens

Commercial polycrystalline copper CuOF 99.95% in initial form of a hot rolled plate of 14 mm of thickness was tested. The specimens were extracted from the centre of the plate and the microstructure of material is presented in Fig.1. The mean grain size was about 30 µm with a lot of annealed twins. The material is quasi-isotropic textured. The present study was conducted by using an ultrasonic fatigue machine at 20 kHz with cylindrical and flat hourglass shaped specimens. The specimen dimensions were calculated so that the free resonant frequency of specimen in the first longitudinal mode is 20 kHz. All specimens were treated at 250°C for 60 min to relieve the residual stress (ASM specialty Hand book) without change of microstructure. Then, a procedure of mechanical and electrolytical polishing was executed till remove all hardened layers on surface specimen. As a result, before testing, the specimens were mirror polished and without residual stresses. The dynamic Young modulus in calculations was E_d = 130 GPa [4]. The stress/strain amplitude along the specimen was estimated by an one-dimensional elastic calculation. It was in a good agreement with the experimental measurement obtained by the strain gages. The geometry and the stress amplitude distribution in specimens are presented in Fig.2.

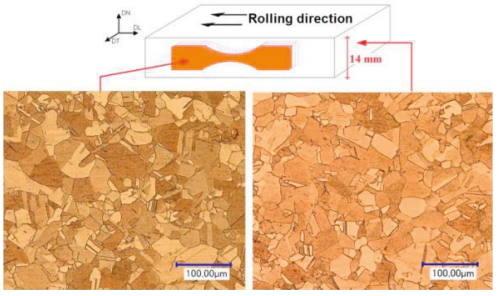

Fig.1. Microstructure of material

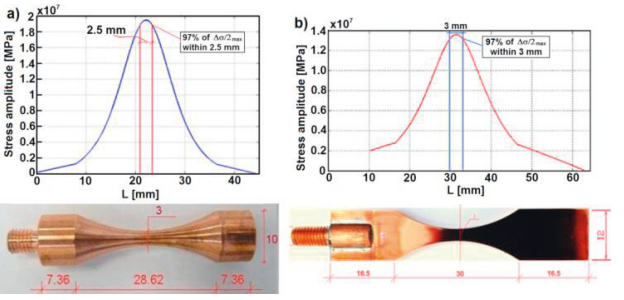

Fig.2. Ultrasonic fatigue specimens
(a) cylindrical specimen (b) flat specimen

2.2 Experimental procedure

To perform experiments up to the VHCF regime, an ultrasonic equipment at a testing frequency of 20 kHz was used. The S-N curve of the material in the VHCF regime was first established. The fatigue tests were carried-out with cylindrical specimens at various stress amplitudes with a constant stress ratio ($\sigma_{max}/\sigma_{min}$) R = -1.

In a previous work [16], the self-heating over ultrasonic fatigue tests was measured by an infrared camera. Figure 3 shows the spatial average of the temperature increase (heating) measured at the surface specimen and the deduced intrinsic dissipation. The temperature increase remains lower than 20°C for stress amplitudes lower than 60 MPa. However it reaches 70°C for higher stress amplitudes. This stronger temperature increase may change properties of copper. That is why in order to prevent from a heating effect at high stress amplitudes, the specimens used for establishing the S-N curve were cooled by a cold air gun during the test till rupture.

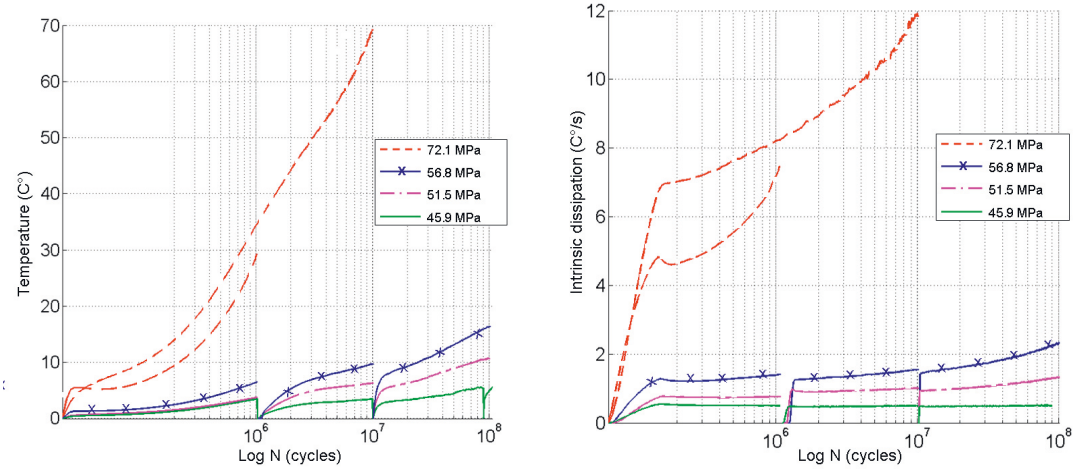

(a) (b)

Figure 3. (a) Average temperature and (b) Average intrinsic dissipation during fatigue test at different constant stress amplitude fatigue test for CuOF 99.95% [16].

To study the formation and development of slip markings on the specimen surface at very low stress amplitudes and after very high numbers of cycles, the flat specimens were used. This type of specimen is appropriate to study the microstructure around the SMs by Electron Back Scatter Diffraction (EBSD) technique and to measure the roughness of SMs by Atomic Force Microscope (AFM) and temperature and intrinsic dissipation by an infrared camera. The experiments were periodically interrupted after several specified numbers of cycles for surface observations. The observations were exclusively made at the centre of the cross section. Indeed, the stress amplitude at the border is lightly greater (~ 5 %) than one at the centre of the cross section.

3. Results

3.1 S-N Curve

The S-N curve of the studied pure copper obtained by using ultrasonic fatigue machine at 20 kHz is shown in Fig. 4. It displays two regimes. In the first regime, failure occured between $3.6x10^6$ and $5x10^7$ cycles with stress amplitude ranging from 115 MPa to 97 MPa. The first regime is associated with the high cycle fatigue (HCF) regime. In the second regime, failure took place at numbers of cycles greater than $5x10^7$ cycles. The stress amplitude is lower than 97 MPa. The S-N curve slope in VHCF is more than 10 times smaller than in HCF (-0.4 MPA/Log(Number of cycles) versus -5.3 MPa/Log (Number of cycles)). In other words, the number of cycles very quickly increases with decreasing the stress amplitude. At $\Delta\sigma/2$ = 91.2 MPa, we did not observe any failure up to $5.4x10^9$ cycles at which the test was stopped. Our results are in very good agreement with Stanzl-Tschegg et al. [4]'s experiment results obtained on similar pure polycrystalline copper. Their results revealed a "fatigue limit at $1x10^{10}$ cycles" also called "fatigue life threshold" equal to at $\Delta\sigma/2$ = 92.2 MPa.

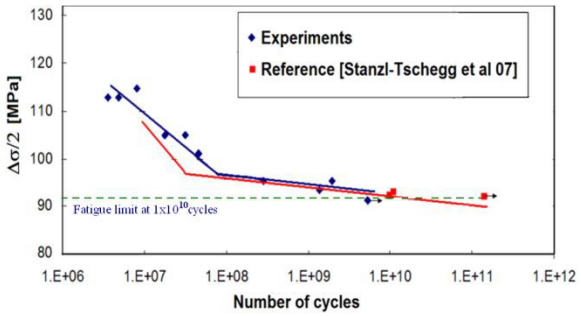

Fig.4. S-N curve of pure copper obtained with ultrasonic fatigue tests

3.2 Three types of slip band in fatigue

The appearance and evolution of slip markings in the VHCF regime for a wide range of stress amplitude from 38 MPa to 115 MPa have been studied. It was found that he lower the stress amplitude, the higher the number of cycles necessary to observe the earliest SMs. Beside, we distinguished 3 types of SMs: type I, type II and type III (Fig.5) which differ from their location within the microstructure and their morphology. All these SMs were shown to be Persistent Slip Markings (PSM), namely when the surface was electropolished after fatigue, the SMs reappeared at the same sites on the specimen surface when fatigue was resumed.

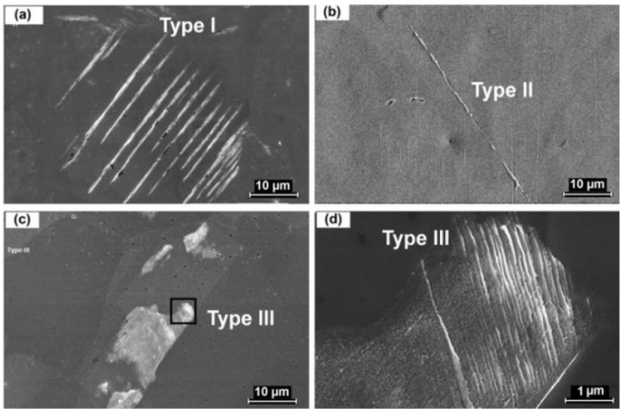

Fig.5. Three types of slip markings in VHCF (a) Type I ; (b) Type II ; (c) Type III and its zoom (d)

3.2.1 Type I

Fig.6 shows SEM images of slip markings type I. They are parallel to each other. They are long, straight and crossing the grain. The width of each SM varies from 0.5 to 3 µm. The distance between the SMs depends on grain size and it is larger for larger grains. It is about 5~7 µm for a grain size of 30 µm (30 µm is the mean grain size of the studied copper). The surface is smooth between the SMs. A quantitative measurement with AFM shows that the height of the extrusions associated with type I SMs is about 0.6 µm and the width is 2 µm (Fig.7). New parallel slip markings appear inside the grain and the height of SM rises with increasing number of cycles.

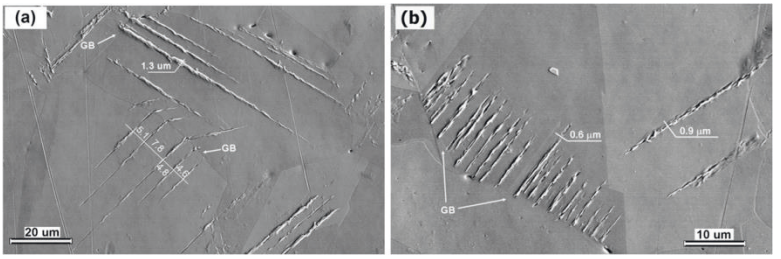

Fig.6. Slip markings type I appeared at $\Delta\sigma/2$ = 89 MPa - 10^6 cycles

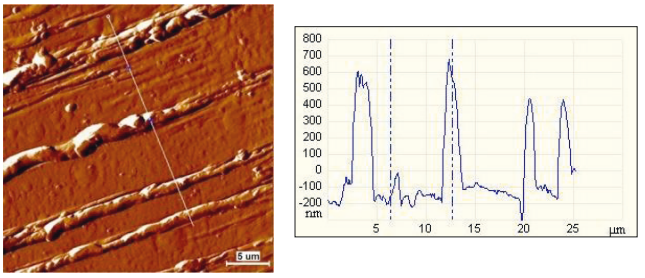

Fig.7. Surface roughness of type I SM at $\Delta\sigma/2$ = 89 MPa - 10^6 cycles (a) AFM image (b) surface profile along the line

3.2.2 Type II

Figure 8a shows examples of SEM micrographs of SM type II. As SM type I, they are long and straight but they are isolated. EBSD image shows that the SM type II was initiated near or typically at a grain boundary (Fig.8.b). The majority of SM type II was formed at twin boundaries. The average height is close to SM type I height (Fig. 9) but the maximum height can reach 1-2µm depending on the stress amplitude and the number of cycles. The initial SMs become longer, larger and higher with increasing the number of cycles. Figure 10 shows the evolution of a type II slip band at $\Delta\sigma/2$ = 55 MPa after 10^7 cycles, 10^8 cycles and $2x10^8$ cycles. This SM was formed at a grain or twin boundary and it grew only in the left grain. No new SM appeared in the close neighborhood of the initial SM.

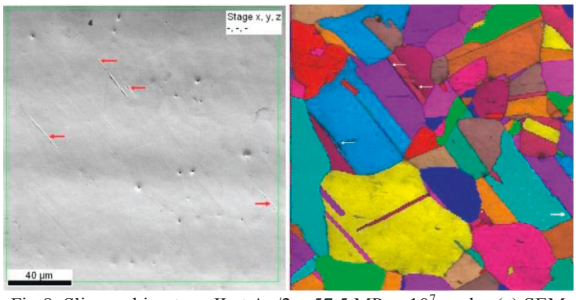

Fig.8. Slip marking type II at $\Delta\sigma/2$ = 57.5 MPa - 10^7 cycles (a) SEM image and (b) EBSD analyze at the same zone shows the appearance of SM type II (arrows) at grain boundary

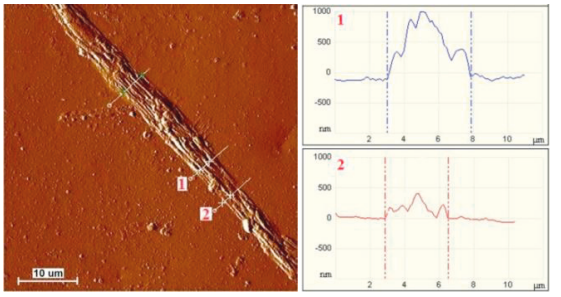

Fig.9. Surface roughness of SM type II
(a) AFM image (b) surface profiles along the lines

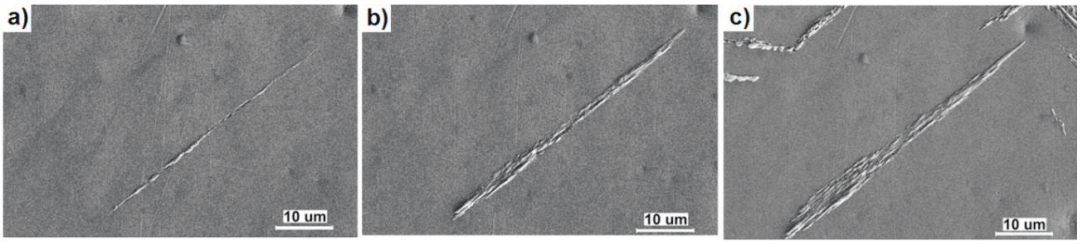

Fig.10. Evolution of SM type II with the numbers of cycles at 55 MPa
(a) after 10^7 cycles ; (b) after 10^8 cycles and (c) after $2x10^8$ cycles

3.2.3 Type III

At the very earliest stages, slip markings of type III are invisible under optical microscopy (MO). SEM observations revealed the presence of clusters of very fine slip markings formed inside the grains and near the grain boundaries. Two slip marking directions were usually observed. The first one is more marked and occupies the majority of the cluster surface. It is very probably associated with the slip band of the primary slip system. The second is less marked and is called "secondary" slip band (Fig.11). Fig.12 shows an AFM image of slip markings of type III at $\Delta\sigma/2 = 50$ MPa after $2x10^8$ cycles. Their roughness is less than 50 nm.

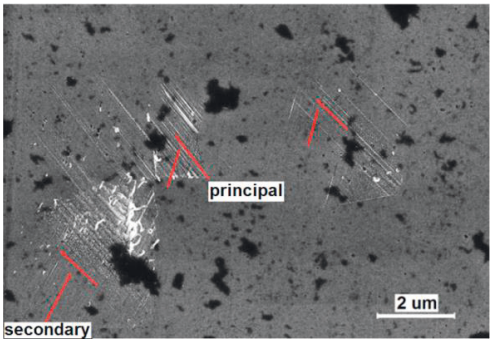

Fig.11.Sslip markings type III at $\Delta\sigma/2 = 48$ MPa after 10^8 cycles with 2 direction of slip

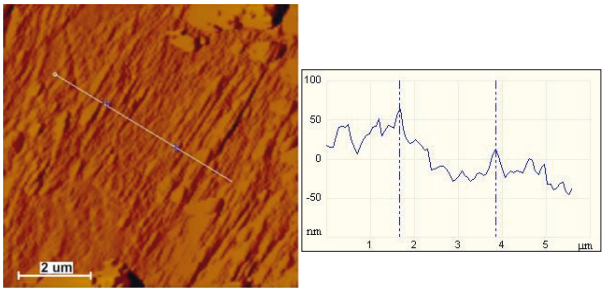

Fig.12. Surface roughness of slip marking type III at $\Delta\sigma/2 =$ 50 MPa after $2x10^8$ (a) AFM image (b) surface profile

3.2.4 Relation between stress amplitude and formation of different types of SM

The appearance of the different types of slip markings depends essentially on stress amplitude. At high stress amplitudes, i.e. higher than "fatigue limit at $1x10^{10}$ cycles" at $\Delta\sigma/2 = 92.2$ MPa, the majority of the first slip markings is of type I. The amount of SM type I decreases with decreasing stress amplitudes and SM type II become more and more dominant. At very low stress amplitudes such as 44 MPa, type III is dominant.

The numbers of cycles necessary to form the earliest SMs and the type of SMs as a function of the stress amplitude are showed in Fig.13. At a given stress amplitude, the test was regularly interrupted to observe the slip markings on the specimen surface. In Fig. 13, the experimental data indicate the last time observation when no slip markings appeared and the next time observation when the earliest slip markings are detected using SEM. Our results are in good agreement with the experimental results obtained by Stanzl-Tschegg and Schönbauer [4]. From 62 MPa to 34 MPa, the stress amplitude varies linearly with the logarithm of the number of cycles necessary to form the earliest slip markings. The S-N curve and the curve for the appearance of the earliest slip bands are compared in Fig.14. Up to 10^8 cycles, at a specified number of cycles, the stress amplitude required to break the specimen is twice larger than the stress amplitude to form the earliest SMs on the specimen surface.

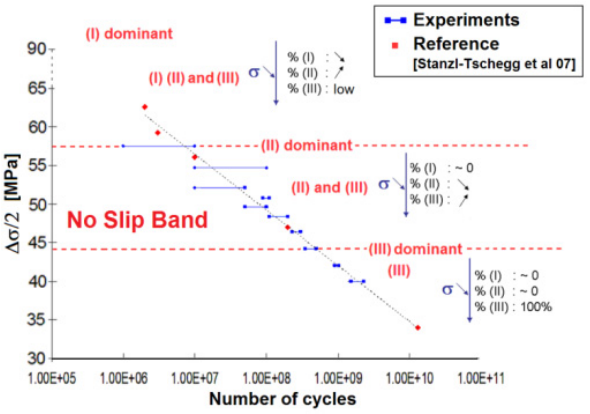

Fig 13. Appearance of the earliest SMs (SBs) –stress-number of cycles curve and types of SMs (SBs)

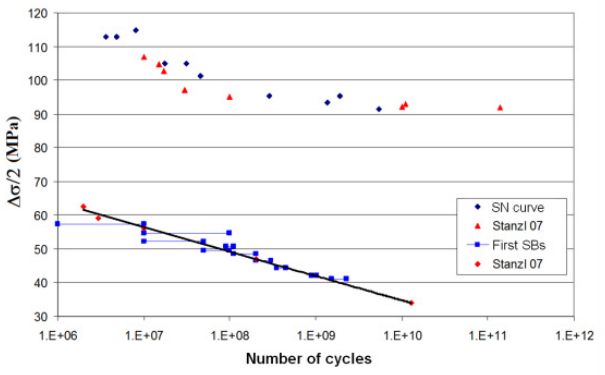

Fig. 14. S-N curves to rupture and to form the earliest slip markings (slip bands)

3.3 Intrinsic dissipation

In a previous paper [17], the average intrinsic dissipation was estimated from thermal field measurements over fatigue tests. Fig. 15 exhibits the intrinsic dissipation d_1 (divided by ρC in order to have volume energy rate (W/m^3) expressed in (°C/s)) at 10^6 cycles for various stress amplitudes ranging from 20 to 90 MPa. Results stressed that dissipated energy exists whatever the applied load. Higher the stress range, higher the intrinsic dissipation. We can note that even below about 30 MPa, at which no slip marking appear even at number of cycles higher than 10^{10} and sometimes considered as an "irreversible threshold" in literature [4], a non-zero intrinsic dissipation can be detected (Fig. 15 (b)). It was also found that dissipation always increased with the number of cycles revealing continuous changes within the material. This result is consistent with the gradual changes of the specimen surface over cycles.

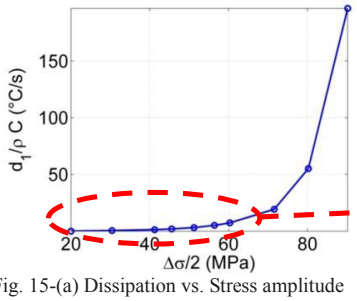

Fig. 15-(a) Dissipation vs. Stress amplitude

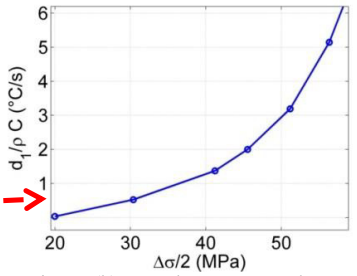

Fig. 15-(b) Zoom between 20 and 60 MPa

3.4 Calculation of the stress field at the surface of a polycrystal

Slip markings of type II and III are localized at or close to grain and twin boundaries. These observations reveal the key role of grain/twin boundaries acting as stress concentration factors. At such low stress amplitudes (with regard to the macroscopic yield stress and fatigue strength), the material is elastic (except at some locations) and the anisotropy of the grain elastic behaviour is responsible for stress heterogeneity and stress concentrations at grain and twin boundaries. To estimate the stress field within the material and to relate it to the sites of SMs, quasi 3D finite element simulations were performed. The real polycrystalline microstructure observed at the specimen surface using EBSD was geometrically represented and discretized (Fig. 16). Four zones of interest (called A, B, C, D) were chosen because they contained SMs of type II. Considering the four zones, the total number of grains is equal to 192. The total number of SM type II is equal to 11. The 2D representations were then extruded in the third direction. Quasi 3D simulations were performed using the ABAQUS software and considering the orientation and the cubic elasticity of each grain. The plastic behaviour is neglected since we are just interested in the earliest SM appearance for which the material is mainly elastic. A uniform compression/tensile uniaxial stress along E_2 axis (specimen axis) was applied on the studied zone boundaries normal to the loading direction. The others surface boundaries were free.

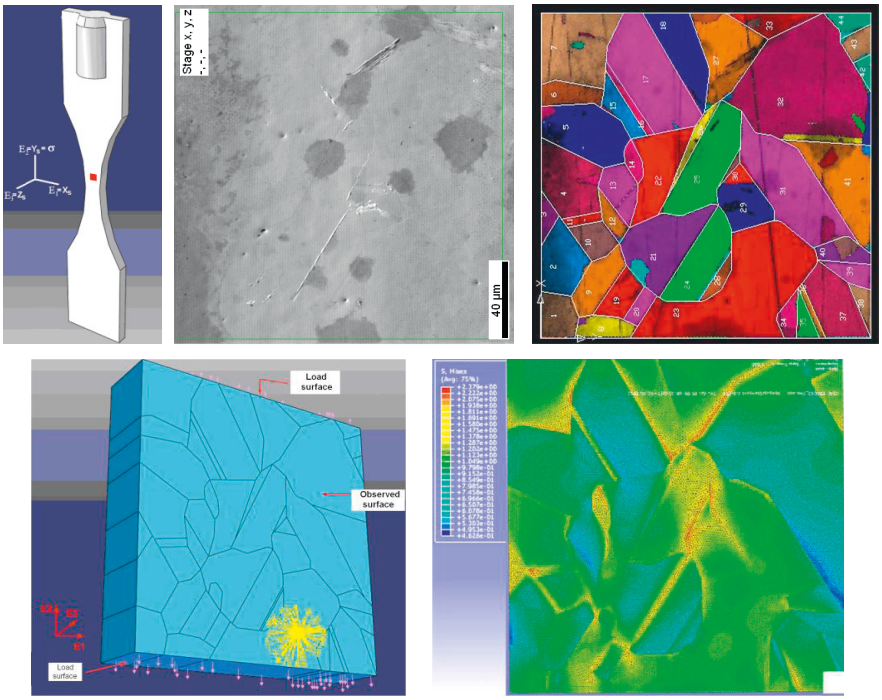

Fig.16. (a) Coordinate system ; (b) SEM image and (c) EBSD image of some type II SB
(d) Simulation on Abaqus ; (e) Von-Mises stress distribution

The Von Mises stress field clearly exhibits stress concentrations at some grain boundaries (Fig. 16 (e)). Copper has a face-centered cubic structure and 12 {111} <110> slip systems. To correlate slip markings and slip systems, the resolved shear stress τ^s on each slip system s was calculated according to the following equation

$$\tau^s = R_{ij}^s \sigma_{ij} \tag{1}$$

where σ is the local stress tensor and R is the Schmid tensor. For each grain, the maximum resolved shear stress was identified and the location at which it was found was noted. For grains displaying one SM type II, the maximum resolved shear stress was systematically found higher close to grain/twin boundaries than within the grain. In some

cases, two very close values were found. To determine the active slip system, we used the marking observed on the specimen surface and measured the π angle. The π angle is the angle between the marking of the slip band and the loading axis (Fig. 17). This measured angle was compared with the calculated one assuming the active slip system. The slip system having one of the highest resolved shear stress and the closed angle π to the experimental one was said to be the active slip system according to the Schmid criterion.

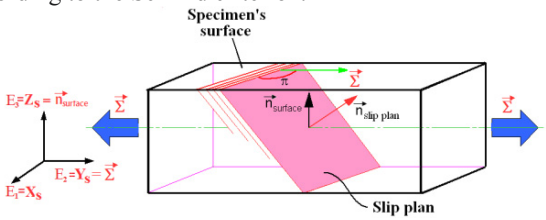

Fig.17. Definition schema of angle π

.

Fig. 18 displays the number of grains (over the 192 grains) having a maximum resolved shear stress divided by the applied stress $|\tau_{max}/\Sigma|$ equal to a given value. The values of $|\tau_{max}/\Sigma|$ range from 0 to about 1. They were divided into intervals of 0.02 except for the first interval which includes values between 0 and 0.35. As mentioned above, 11 grains over the 192 grains exhibited one slip marking. These grains are indicated by the following notation: G Number of the grain / Label of the zone (A, B, C or D). For example, G32/A means a slip marking in the numbered 32 grain belonging to the A zone. In addition, the maximum Schmid factor was calculated for each grain. Note that the maximum Schmid factor is also the ratio of the maximum resolved shear stress over the applied stress $|\tau_{max}/\Sigma|$ for which the maximum resolved shear stress is calculated assuming a uniform stress state ($\sigma=\Sigma$), in other words isotropic elasticity. To sum up, the number of grains having $|\tau_{max}/\Sigma|$ of a given value and calculated assuming isotropic and anisotropic elasticity was plotted as a function of $|\tau_{max}/\Sigma|$ (Fig. 18). Note that, while the Schmid factor is bounded between 0 and 0.5, $|\tau_{max}/\Sigma|$ calculated assuming anisotropic elasticity reaches 1 because of the stress concentration or/and triaxiality.

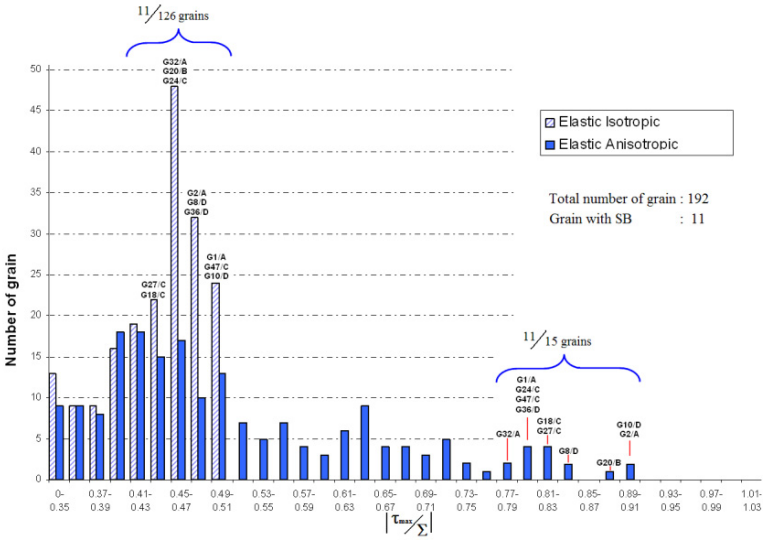

.

Fig.18. $|\tau_{max}/\Sigma|$ calculated assuming isotropic or anisotropic elasticity for the 192 grains contained in zones A, B, C and D. 11 grains contained one slip marking type II.

The Schmid factor ($|\tau_{max}/\Sigma|$) for the grains having one slip marking ranges from 0.44 and 0.5. However, many other grains (115 grains) which do not have any slip marking also have a maximum Schmid factor between 0.44 and 0.5. This result demonstrates that considering the maximum Schmid factor is not a good criterion to predict

the grains having one SM type II. In addition, it cannot predict the location of the marking since $|\tau_{max}/\Sigma|$ is uniform within a grain.

The $|\tau_{max}/\Sigma|$ values, calculated assuming anisotropic elasticity, for the grains having one slip marking ranges from 0.78 and 0.9. In that case, only 4 other grains have their $|\tau_{max}/\Sigma|$ value in this range and do not have any slip band. This result show that considering the maximum $|\tau_{max}/\Sigma|$ is a good criterion to predict the grains having one type II slip band: it predicts more than 70% of grains having one slip band type II. In addition, it predicts the location of the band.

The previous analysis also revealed that the 11 slip bands are located at or very close to a grain boundary whose disorientation is very high from 58.5 ° to 60 °. 9 of these bands appeared at or very close to a twin boundary. The associated slip plane is a plane parallel to the plane of the twin boundary (G1/A, G2A, G32/A, G20/B, G18/C, G28/C, G47/C, G36/G10 and G10/D). For The last two slip bands (G27/C and G8/D), the grain boundary is not a twin boundary, although the disorientation between the two grains is close to 60°. This result proves that twin boundaries are preferred location for appearance of slip markings (slip bands) in fatigue at very low stress amplitudes.

4. Discussion and conclusion

In LCF and HCF regime, the crack initiation in high purity polycrystalline metal mainly occurs along PSBs crossing the grains (type I). PSBs appear in well-oriented grains for plastic slip and are generally along one dominant direction given by the primary slip system. An analysis based on the maximum Schmid factor (and so which does not take into account the elastic anisotropy) predicts well the grains which have PSBs and the active primary slip system [18-19]. In the VHCF regime, it was shown that slip marking of type II perfectly correspond to slip bands associated with a primary slip system. An analysis based on the maximum resolved shear stress (Schmid criterion) is relevant as soon as the stress heterogeneities due to elastic anisotropy are considered. Such a criterion predicts the location and the active primary system of the slip band type II. Similar investigations on slip markings type III are ongoing. Literature results demonstrate the role of twin boundaries for crack initiation [20-21]. Very few works were dedicated to the relationships between slip bands and twin boundaries. They rather focused on the role of disorientation [22]. In this paper, the key role of twin boundaries on the slip band type II was proved for pure copper specimens loaded in the VHCF regime. Slip markings were found to continuously change over the cycles. Consistently, the dissipation always increased with the number of cycles even at stress amplitudes at which no slip marking was visible at 10^{10} cycles. These results raise the question of the existence of a fatigue limit for pure copper.

Acknowledgements

The authors are grateful for financial support from Agence Nationale de la Recherche France ANR-09-BLAN-0025-01 and to company Griset for supplying copper. The authors thank also very much Professor Haël Mughrabi for the scientific discussions.

Bibliography

[1] Bathias C. and Paris P. (2004) Gigacycle fatigue in mechanical practice. CRC Press, 1st edition

[2] Mughrabi H, Wang R. Cyclic stress–strain response and high-cycle fatigue behaviour of copper polycrystals. In: Luka´s˘ P, Pola´k J, editors. Basic mechanisms in fatigue of metals. Academia and Amsterdam, Prague: Elsevier; 1988. p. 1–13.

[3] Mughrabi H. - Specific features and mechanisms of fatigue in the ultrahigh-cycle regime - International Journal of Fatigue 28 (2006) 1501–1508.

[4] Stanzl-Tschegg S, Schönbauer B. PSB threshold and fatigue limit of polycrystalline copper in the VHCF-regime. In: Allison JE, Jones JW, Larsen JM, Ritchie RO, editors. Proceedings of fourth international conference on very high cycle fatigue (VHCF-4). USA: TMS; 2007. p. 15–22.

[5] Weidner Anja, Amberger Dorothea, Pyczak Florian, Schönbauer Bernd, Stanzl-Tschegg Stefanie, Mughrabi Hael, Fatigue damage in copper polycrystals subjected to ultrahigh-cycle fatigue below the PSB threshold - International Journal of Fatigue (2009)

[6] Stanzl-Tschegg S. E., Schönbauer B. - Mechanisms of strain localization, crack initiation and fracture of polycrystalline copper in the VHCF regime - International Journal of Fatigue 32 (2010) 886–893
[7] Cretegny L. and Saxena A., AFM characterization of the evolution of surface deformation during fatigue in polycristalline copper, Acta mater. 49 (2001) 3755–3765, 2001
[8] Huang H.L., N.J. Ho ,The study of fatigue in polycrystalline copper under various strain amplitude at stage I: crack initiation and propagation, Materials Science and Engineering A293 (2000) 7–14
[9] Lukas P., Klesnil M. and Polak J. - High Cycles Fatigue life of metals - Materials Science and Engineering, 15 (1974) 239 – 245.
[10] Mughrabi H, On multi-stage fatigue life diagrams and the relevant life controlling mechanisms in ultrahigh-cycle fatigue. Fatigue Fract Engng Mater Struct 2002;25:755–64.
[11] Pommier S., 'Arching' effect in elastic polycrystals: implications for the variability of fatigue lives, Fatigue & Fracture of Engineering Materials & Structures25 (2002) 331–34
[12] Sauzay M., Cubic elasticity and stress distribution at the free surface of polycrystals, Acta Materialia, 55 -2007) 1193-1202
[13] Winter AT, Pedersen OB, Rasmussen KV (1981) Dislocation microstructures in fatigued copper polycrystals. Acta Metallurgica 29:735–748
[14] Mareau C., Favier V., Weber B., Galtier A., Berveiller M., Micromechanical modeling of the interactions between the microstructure and the dissipative deformation mechanisms in steels under cyclic loading, International Journal of Plasticity, 32-33, 106-120, 2012
[15] Mareau C., Favier V., Weber B., Galtier A., Influence of the free surface and the mean stress on the dissipation in steels under cyclic loading, International Journal of Fatigue, 31, 1407–1412, 2009
[16] Favier V., Phung N.L., Ranc N., Bretheau T., Groslafaige J., Roger G., Seiler W., Valès V., Wagner D., Wang C., Bathias C., Cédelle J., Ranc I., Chrysochoos A. , Blanche A., Wattrisse B., Camp G., Clary A., El Kaim Y., Jourdan F., Grégori F., Bacroix B., Galtier A., Thoquenne G., Mughrabi H., Microplasticity and energy dissipation in very high cycle fatigue, Fatigue Design, Senlis, CD-ROM 2011
[17] Blanche A., Ranc N., Chrysochoos A., Favier V., Dissipation measurements in dynamic high cycle fatiguein copper during VHCF loading, Photomechanics, Montpellier, 2013
[18] Blochwitz C, Brechbu¨ hl J, Tirschler W. Analysis of activated slip systems in fatigued nickel polycrystals using the EBSD-technique in the scanning electron microscope Mater Sci Eng A 1996;210:42
[19] El Bartali, Aubin V.; Sabatier L.; Villechaise P.; and Degallaix-Moreuil S. - Identification and analysis of slip systems activated during low-cycle fatigue in a duplex stainless steel, Scripta Materialia 59 (2008) 1231–1234.
[20] Neumann, P. & Tonnessen, A (1988) Crack initiation at grain boundaries in FCC materials – Strength of Metals and Alloys vol 1, pp 748-8 Oxfoxd: Pergamon Press
[21] Thompson N., Wadsworth N. & Louat N., The origin of fatigue fracture in copper., Phil. Mag. A, Vol. 1, 1956, pp. 113–126.
[22] Kim, W. H. and Laird, C., *Acta metall.*, 1978, **26**, 777, 789